NUCLEOLAR DYNAMICS: REARRANGEMENT OF NUCLEOLUS ASSOCIATED CONDENSED CHROMATIN UNDER DNA DAMAGE INDUCED BY DIFFERENT DOSES OF γ-IRRADIATION

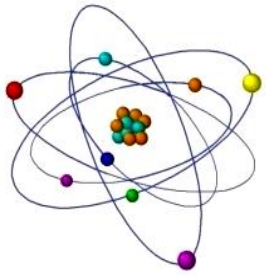

[1,2]Lili Nadaraia, [1]Vera Okuneva, [3]Mikheil Gogebashvili, [3]Nazi Ivanishvili, [1]Pavel Tchelidze*

[1]Carl Zeiss Education and Scientific Center, New Vision University, Georgia
[2]Republic Center of Structure Research, Georgian Technical University, Georgia
[3]I.Beritashvili Center of Experimental Biomedicine, Laboratory of Radiation Safety Problems, Georgia

*Corresponding author: pavel.tchelidze@univ-reims.fr

ABSTRACT: *The nucleolus, a vital nuclear compartment, orchestrates ribosome biogenesis by producing polycistronic transcripts. It integrates gene-rich chromosomal domains, forming nucleolus-associated DNA (naDNA) or nucleolus-associated chromatin (NAC). The nucleolus hosts molecular machinery that guides the transcription of ribosomal genes (r-genes), pre-rRNA processing, and ribosome assembly. These are organized into nucleolar components (NCs). NAC, consisting of intra-nucleolar condensed chromatin (ICC) and peri-nucleolar condensed chromatin (PCC), is less studied, and its functional significance in establishing and maintaining the global nucleolar structure still needs to be elucidated. Previous studies demonstrated the spatiotemporal reorganization of NAC by inhibiting rRNA synthesis with DNA intercalating compound - actinomycin D (AMD), leading to profound changes in ICC and PCC. This study explores the structural reorganization of NAC under severe DNA damage induced by γ-irradiation. The focus is on ICC and PCC to investigate whether physically damaged naDNA retains the ability to move/contract, similar to the chemical inhibition observed with AMD. Histone H2B-GFP permanently transfected He-La cells were utilized for their stability and suitability for time-lapse imaging. γ-Irradiation was applied at 10 Gy (Gray) and 30 Gy doses, followed by post-irradiation imaging for 24-72 hours. Two approaches were employed: post-irradiation LSM imaging of fixed and living cells (time-lapse LSM). The structural organization of NAC, ICC network, and PCC shell were analyzed to understand the spatial changes induced by γ-irradiation. The study reveals that γ-irradiation-induced NAC inactivation dynamics mirror changes observed with AMD-induced rRNA synthesis inhibition. Under both regimes (10 Gy and 30 Gy) of γ-irradiation, ICC structures coalesce, forming more significant and more prominent clumps that migrate toward the PCC shell. This research provides insights into the dynamics of nuclear and nucleolar changes induced by severe DNA damage. The observed similarities between chemical inhibition and γ-irradiation effects on nucleolus-associated chromatin emphasize its significance in nucleolar organization. The study contributes to understanding the spatial changes in nucleolar structure under different modes of cellular stress.*

Key words*:* Nucleolus – Nucleolar Components – Nucleolus Associated Chromatin – γ-Irradiation

INTRODUCTION

The nucleolus, a key nuclear compartment, drives ribosome biogenesis by generating polycistronic transcripts, namely the 47S precursor or pre-rRNA. Through cleavage during processing, it yields the final forms of rRNAs - 18S, 5.8S, and 28S, while their maturation and assembling processes lead to the formation of pre-ribosomal sub-particles. Integrating gene-rich chromosomal domains, it forms giant tandems of eukaryotic rDNA loops comprising numerous r-gene repeats. This process, facilitated by accessory protein factors, forms naDNA domains known as NAC. The nucleolus houses extremely compact yet highly active molecular machinery orchestrating ribosomal r-genes transcription, pre-rRNA processing, and pre-ribosomal assembling [1-13].

In the nucleolar realm, molecular machinery intricately orchestrates ribosome biogenesis within tightly coordinated NCs, functional sub-compartments discernible in light and transmission electron microscopes (LM and TEM). These NCs, marked by specific protein signatures, structurally organize transcription and processing machinery into three major NCs. This tripartite nucleolar structure is exceptionally identifiable in TEM by its distinct ultra-structural appearance and electron density. Transcriptionally active, non-nucleosomal ribosomal chromatin (r-chromatin) takes the form of pale-stained fibrillar centers (FCs), recognized as an interphase counterpart of mitotic nucleolus organizing regions (NORs). Two additional NCs, the dense fibrillary (DFC) and the granular component (GC), represent early and late processing sub-compartments. Here, 47S pre-rRNA molecules undergo maturation steps, leading to the generation of 40S and pre-60S particles containing precursors to 18S, 28S, 5.8S, and 5S rRNAs. The transitional area between r-genes transcription foci—termed transcriptionally active r-genes territory - is situated between the FC surface and the surrounding DFC [1-13]. In active nucleoli, the products of pre-rRNA synthesis, processing, and pre-ribosome assembly cluster around numerous r-chromatin transcription foci, thus shaping the multifocal global organization of the nucleolus.

Meanwhile, naDNA or NAC domains, though less explored and not determined by the genome map, likely contain more than just r-genes [9-22]. Therefore, these chromatin-associated NCs, with undefined roles in nucleolar organization, are intriguing. NAC manifests as a shell of PCC (PCC shel) extending into strands of ICC (ICC network). ICC is observed in EM-light zones known as nucleolar vacuoles (NVs). On ultrathin sections, ICC and PCC, constituting 10-30 nm thick nucleosomal fibrils, form a single interstitial/vacuolar network system. 3D reconstruction reveals that FCs are intricately linked via ICC clumps [23-26]. Previous studies using the rRNA synthesis inhibitor AMD showcased NAC spatiotemporal reorganization. AMD selectively blocks rRNA synthesis in low concentrations (0.05 μg/ml), causing giant FCs, DFC zones, and large ICC clumps. This approach demonstrated the inactivation dynamics of rRNA synthesis, revealing stepwise gathering and fusion of FCs and NAC. This concerted contraction mobilizes nucleolar components. The tight link between FC and DFC, displaced by selective r-genes transcription block, resembles FC/DFC assembly movement. Time-lapse imaging elucidates FC/DFC assembly dynamics, attributed to progressive NAC condensation in response to r-genes transcription inactivation.

The physical bond between FCs and ICC propels the movement of the FC/DFC complex,

aligning with NAC constituent inactivation dynamics [27].

Having explored NAC inactivation dynamics through chemical r-genes transcription inhibition, we now delve into the structural reorganization of NAC under severe DNA damage by physical factor γ-irradiation that induces single-strand breakages [28-34]. Focusing on ICC and PCC, we investigate if physically damaged naDNA exhibits similar movement to that induced chemically. Our preferred model involves possible post-γ-irradiation (10 Gy and 30 Gy) nucleolar inactivation monitoring changes in He-La cells permanently expressing histone H2B-GFP over 24-72 hours. We utilize LSM 2D imaging and LSM time-lapse analysis to scrutinize how nuclear and nucleolar structures, including naDNA, adapt to large-scale DNA damage. Based on chemical inhibition studies, our hypothesis posits that γ-irradiation induces classical spatial changes akin to NCs segregation [27, 35-39]. Indeed, our findings demonstrate NAC inactivation during γ-irradiation mirroring those observed with AMD-induced rRNA synthesis inhibition. Both regimes (10 Gy and 30 Gy) show the ICC network gradually coalescing before migrating towards the PCC, eventually fusing and forming more significant, more pronounced ICC clumps.

MATERIAL AND METHODS

1.Cell Culture

In our investigation of NAC distribution changes during irradiation, we utilized histone H2B-GFP transfected He-La cells obtained from Prof. O. Piot (University of Reims Champagne-Ardenne, France). The choice of this cell line was based on:

- **Stability:** The nuclear fluorescence of these cells demonstrated high stability, crucial for obtaining brightly fluorescent, reliably transfected cells, especially during time-lapse imaging of post-radiated cell dynamics.
- **Intra-nucleolar Fluorescence:** These cells exhibited prominent intra-nucleolar fluorescence, identified as nucleosomal domains with the ultrastructural appearance of ICC. This characteristic was vital for our study.
- **Distinct Features:** He-La cells are known for their large FCs associated with prominent DFC zones, aiding in the discrimination of nucleolar sub-territories involved in r-gene transcription and pre-rRNA processing.

Cell Maintenance: Stock cultures were maintained in 40 ml flasks containing DMEM (Gibco, UK) supplemented with 10% calf serum and 1% penicillin/streptomycin mixture. Regular reseeding occurred 2-3 times per week based on the cell monolayer reaching late pre-confluent or early confluent stages. Monthly tests for mycoplasma detection were conducted.

Preparation for Post-Irradiation Imaging: To study ICC dynamics during γ-irradiation-induced nucleolar remodeling, we prepared He-La cells expressing histone H2B-GFP. We ensured cultures remained sub-confluent after 48-72 hours of post-irradiation incubation and/or post-irradiation acquisition of living cell images.

2. Cell Seeding Methods

Method (1): The collagen-coated glass surface of Ø35 mm "MatTek" Petri dishes, featuring 14 mm wells as the growth area (MatTek, USA), was pre-conditioned by pouring a few drops of media at 37°C for 15-30 minutes. The exact amount of meticulously homogenized cell suspension was added. Cell density and distribution were checked using a phase-contrast regime after incubation at 37oC for 15-30 min. The satisfactory density of cells within the growth area was obtained by dilution that yielded ~10.000-15.000 cells/ml. Medium (1.5-2 ml) was added by pouring on the wall of Petri dishes to avoid disturbing the attached cells. Cells can be repeatedly re-homogenized inside the well using a 1.0 ml pipette/syringe. Using this concentration, we regularly achieved a dispersion of ready-to-work cultures after 48 hours of incubation. Following these conditions, we obtained cultures showing attached/flattened cells gathered in small groups distributed sparsely enough to stay sub-confluent after 72 h.

Method (2): This method yielded a less dispersed pattern, yet suitable for maintaining sub-confluence after 72 hours. The collagen-coated glass surfaces were pre-conditioned, as described above. 1.5-2.0 ml of a properly homogenized cell suspension (~10.000-15.000 cells/ml) was poured into wells. Desired dispersion was achieved by agitation for 5 minutes. Repeated resuspension with a 1 ml pipette/syringe provided better dispersion.

Both methods ensured the availability of isolated cellular groups suitable for post-irradiation incubation and imaging. After 24-48 hours of incubation, cells were briefly rinsed with PBS and prepared/submitted for γ-irradiation by incubating in a fresh medium at 37°C for 2-3 hours.

3. Experimental Procedures for Time-Lapse Imaging, Data Analysis and Visualization γ-Irradiated Cells

Before being submitted to γ-irradiation, cells were briefly rinsed with PBS (3 times during 5 min), immersed in fresh medium, and the dishes were delivered to "GUPOS" γ-installation. Irradiation of cells was conducted directly in Petri dishes at a temperature of 35+/- 2^{o}C. As a source of γ-irradiation, the Cs^{137} isotope with a dose of 1.1 Gy/min has been utilized. After irradiation, cells were washed in PBS (3x5 min), returned to the cultivation media, and then s γ-installation subjected to time-lapse imaging during 0-72 h using Carl Zeiss (Germany) LSM 900 microscopes equipped with Axio Observer Z1/7 inverted microscope and AiryScan 2 augmented resolution device. All procedures, including post-irradiation behavior observation, were conducted on cultures directly in Petri dishes. The imaging was performed at 37°C in a CO_2-enriched atmosphere using a special microscope plate holder with a sealed box. Microscopy details included using various objectives at optical zooms of 100x, 200x, and 630x. Hence, images were registered at low and high magnifications using objectives with corresponding numerical apertures. We used Plan-Neofluar/10x with 0.3 M27 numerical aperture and Plan-Apochromat/20x/0.8 M27 for low magnification, including a time-lapse approach. By imaging objects at high magnification, including time-lapse mode, we used Plan-Apochromat/63x/1.4 Oil DIC M27. The time-lapse imaging setup involved capturing images every 10 minutes for every 24 h post-irradiation imaging time (i.e., 0-24h, 24-48, and 48-72 h), simultaneously in phase contrast and fluorescence regimes.

Histone H2B-GFP fluorescence was induced and recorded using a Colibri 7 laser device at 488 nm excitation light, while emission light was 517 nm. As a control, we used high-magnification

LSM imaging conducted before γ-irradiation treatment. For time-lapse analysis and visualization behavior of living cells damaged by γ-irradiation, obtained time series were transformed into 2D movies using ZEN3.0 software. Significant points from the dataset were extracted to visualize the changes in nuclear/nucleolar quantitative and structural parameters, as well as the movement and coalescence of ICC clumps during γ-irradiation.

RESULTS

1. Exploring γ-Irradiation Induced Nuclear/Nucleolar Changes in Histone H2B-GFP He-La Cell: Fixed Cell Imaging and 2D Time-Lapse Dynamics

The He-La culture, expressing histone H2B-GFP, was selected for its bright, UV-resistant nucleoplasm and intra-nucleolar fluorescence, enabling extended LSM observations with minimal photo-bleaching for up to 24 hours. This resistance proved crucial for living cell observations. Notably, the nuclear chromatin and ICC exhibit early apoptosis-associated changes, making this culture suitable for cellular stress experiments induced by chemical and/or physical factors. By targeting the entire nucleoplasm and ICC, which express histone H2B-GFP fluorescence indicative of condensed chromatin, we investigated structural modifications during the 2D-time series. Therefore, these cells serve as a convenient model to assess the potential drastic effects of γ-irradiation on cell viability, morphology, and physiology.

LSM images displayed in Figure 1. and Figure 2. reveal the structural organization of histone H2B-GFP He-La cell nuclei in fixed control cells. Typically, 2D observations show mononuclear cells, as revealed by merging of phase contrast and fluorescent images (Figure 1. a). Predominantly nuclei have roundish or ovoid shape with smooth contours, while an average diameter ranged between ~14-18 µm (Figure1. b-d). Abundant dividing cells being at different stages of mitosis and occasional apoptotic cells (Figure 1. d) are also seen (Figure 1. a, b, d). Brightly fluorescent nucleoplasm, ICC, and PCC are prominently featured. Nucleoli, are well recognizable as roundish dark zones that have a diameter ranging from ~4-6.5 µm. Even at low magnification, it became obvious that nucleoli contain histone H2B-GFP positive structures of different sizes and appearances attributed to ICC. ICC inclusions have slightly less intense labeling than chromatin fluorescence (Figure 1. a-d).

These features become evident by analyzing various individual/random 2D sections at higher magnification. Therefore, Figure 2. displays the 2D structure, sizes, and localization of the ICC network and the closely adjacent PCC ring. The ICC zones are prominent and vary in size, appearing in individual sections as distinct clumps or extended anastomosing cords. PCC consistently exhibits higher fluorescence than ICC, forming around confines of the nucleolar territory quite thick, solid, or locally disrupted "ring" of ~0.25- 0.55 µm" in thickness (Figure 2. a-d). Therefore, high-magnification images confirm the persistent presence of numerous ICC inclusions and ring-shaped PCC in all observed cells. ICC is either visible as discrete entities or forming well-recognizable network-like structures (Figure 2. c). Furthermore, the analysis at higher magnification confirmed that PCC is organized into a locally open ring. However, it covers a significant part of the nucleolar territory. In addition, these images provide definitive evidence confirming the direct physical link between the PCC ring and ICC clumps as reported

earlier from observations on random ultrathin sections, including those treated for preferential demonstration of NAC [23-25]. Indeed, 2D information presented in Figure 2. b-d reveals multiple cord-like structures emanating from the PCC ring. These "off springs" protrude inside the nucleolar territory, sometimes creating the impression of discrete ICC clumps on individual sections. These findings strongly support the existence of a united ICC network that is continuous with the PCC ring, representing protrusions of the latter.

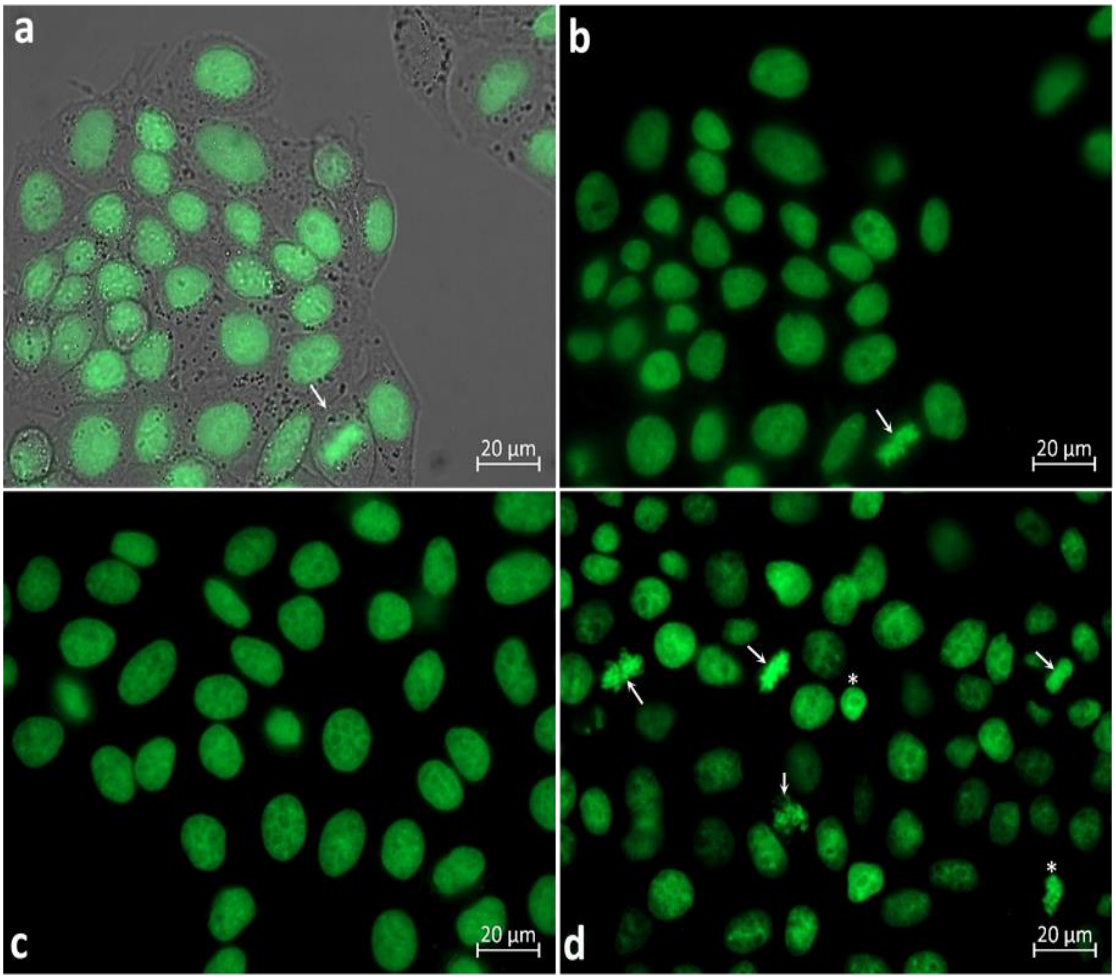

Figure 1. Gallery of images displaying general morphology of fixed cultured He-La cells permanently expressing histone H2B-GFP fused protein. Images were taken at low magnification using phase contrast and fluorescent imaging; a – overlay of phase contrast and fluorescent images demonstrated in order to discriminate mono- and polynuclear cells. All registered cells are mononuclear; b-d – predominantly roundish and/or ovoid shape as well as nearly smooth nuclear contours are better recognizable by fluorescent regime. Nucleolar territory appears in form of roundish or elongated intra-nuclear zone with obviously less intense fluorescence. Even at low magnification it become visible that nucleolar territory is surrounded by ring of PCC, while intra-nucleolar fluorescence is conditioned by presence of worst recognizable ICC structures. Mitotic cells are abundant (Figure 1. a, b, d, arrows) while occasional apoptotic cells are also present (Figure 1. d, marked by stars).

Meanwhile, fixed cells lost about 25%-30% of their initial volume, likely due to shrinkage resulting from PAF fixation. Therefore, we performed time-lapse imaging to capture the 2D dynamics of the NAC, consisting of a PCC ring in continuity with ICC strands in native state (Figure 3.). Analysis of random 2D sections obtained during time-lapse imaging replicated the observed fixed cell pattern, with minor differences in sizes of structures of interest (SOI) between fixed and living cells (Figure 3. a, b) However, we noted that average diameter of nuclei in living He-La cells is higher than in fixed ones and ranged between 17-21 µm. In addition, SOI in fixed cells exhibited fluorescence comparable to or slightly less intense than that in living cells. Random 2D images of living cells prominently revealed all SOI, namely ICC and PCC (Figure 3. c, d). Nucleolar sizes were also slightly higher than in fixed cells, reaching 6.25-8 µm. Living cells were rich in discrete histone H2B-GFP-positive labeling within the nucleolar territory. As expected, ICC appeared as larger clumps or anastomosing cords that form network-like structures (Figure 3. c, d). Accordingly, we can conclusively state that the native structure of ICC is network-like. The extensively branched ICC network consists of anastomosing cord-like protrusions emanating from the PCC shell. Meanwhile, the PCC resembles a highly compacted part of the juxta-nucleolar nucleoplasm, forming a ring delineating the nucleolar territory.

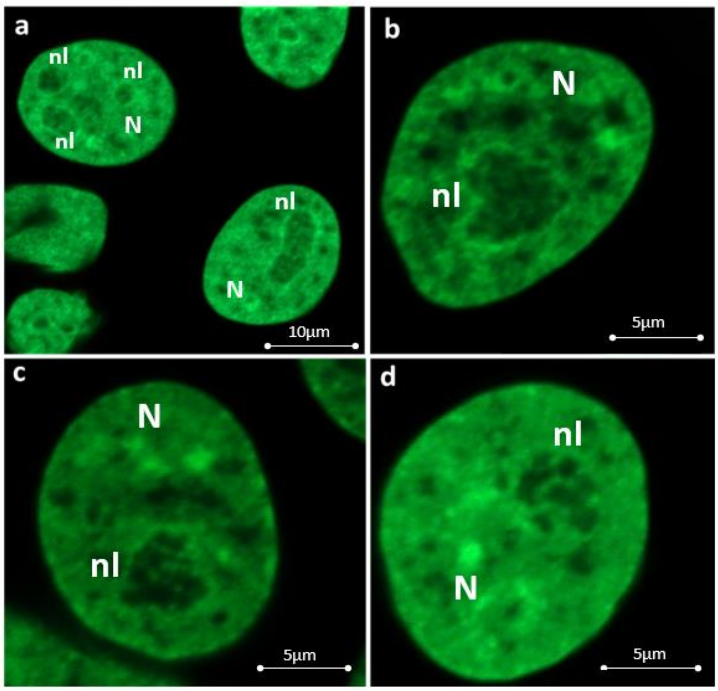

Figure 2. Morphology of nuclei in fixed histone H2B-GFP permanently transfected He-La cells taken at higher magnification; a – medium magnification, general view; note abundant intra-nucleolar GFP-positive inclusions revealing network-like appearance. Note also profound PCC surrounding nucleolus in form of solid ring; b-d – undoubtedly at higher magnification ICC structure became much more prominent, showing either network-like organization (Figure 1. b) or looking as clumps (Figure 1. c). In all samples one can recognize cords of different thickness emanating from prominent PCC ring. This phenomenon is especially well pronounced on Figure 2. d, where interconnected with PCC coarse ICC cords are clearly seen. N –nucleus; nl - nucleolus

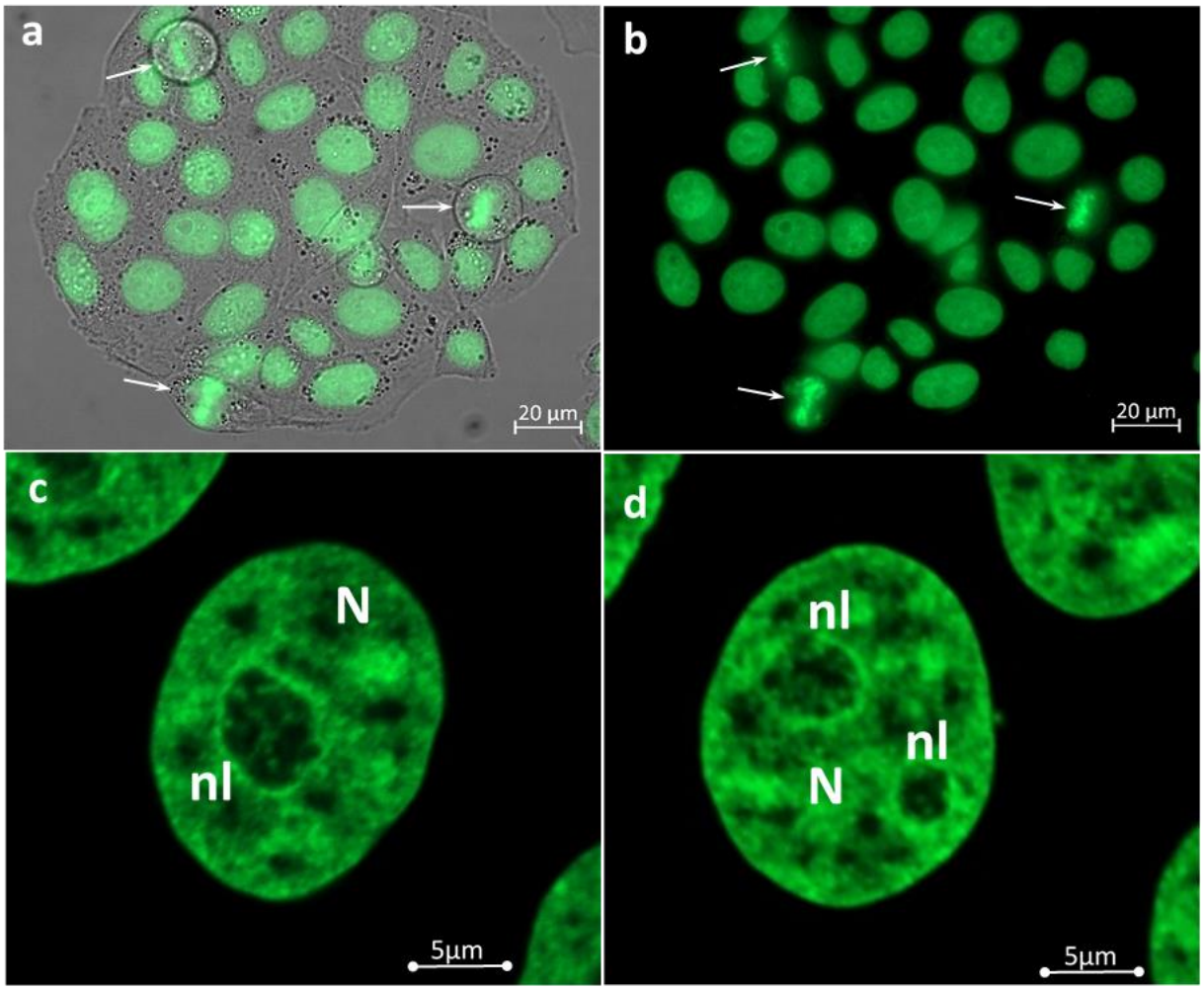

Figure 3. Morphology of cells and nuclei in living histone H2B-GFP permanently transfected He-La cells taken at low (Figure 1. a-b) and high (Figure 1. c, d) magnification; a, b – general view; a - overlay of phase contrast and fluorescent images to reveal mono- and polynuclear cells. All cells are mononuclear and predominantly roundish and/or ovoid. Note abundant mitoses (Figure 3. a, b, arrows); c-d – similarly to fixed cells at high magnification intra-nucleolar GFP-positive inclusions revealing network-like appearance. Note also profound PCC surrounding nucleolus in form of solid ring and emanating from PCC ICC cords. N –nucleus; nl - nucleolus

1.1. Visualizing Nuclear/Nucleolar, ICC and PCC Dynamics: Time-lapse Imaging of He-La Cells Under γ-Irradiation

Time-lapse imaging of He-La cells expressing histone H2B-GFP was conducted to study the dynamics of DNA-containing SOI under γ-irradiation at 10 Gy and 30 Gy. This approach facilitated simultaneous imaging of whole nuclei and nucleoplasm, allowing for 2D analysis of modifications over time. Time series images registered at various time points were used to create galleries of random/individual sections.

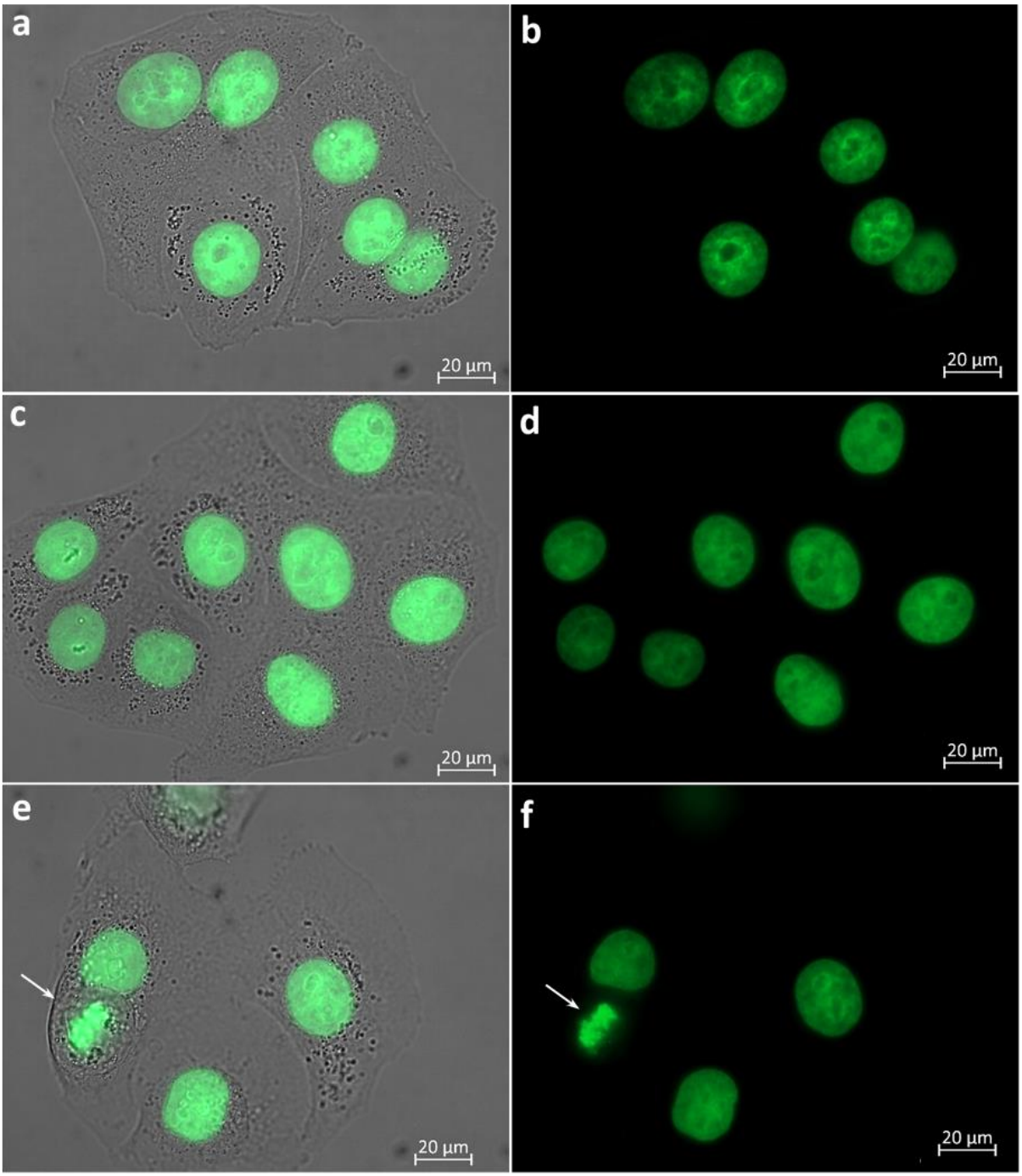

Figure 4. Cellular and nuclear morphology in living histone H2B-GFP permanently transfected He-La cells after irradiation with 10 Gy taken over 48 h; a-f – medium magnification; a, c, e - overlay of phase contrast and fluorescent images; b, d, f – same cells demonstrated in fluorescent regime only. All registered cells remain mononuclear, while nuclei maintain predominantly roundish and/or ovoid shape and smooth contours. Intra-nucleolar GFP-positive inclusions become sufficiently prominent (Figure 4. a-d). Note profound PCC surrounding nucleolus in form of solid ring (Figure 4. b). Also note presence of mitotic cell (Figure 4. e, f, arrows).

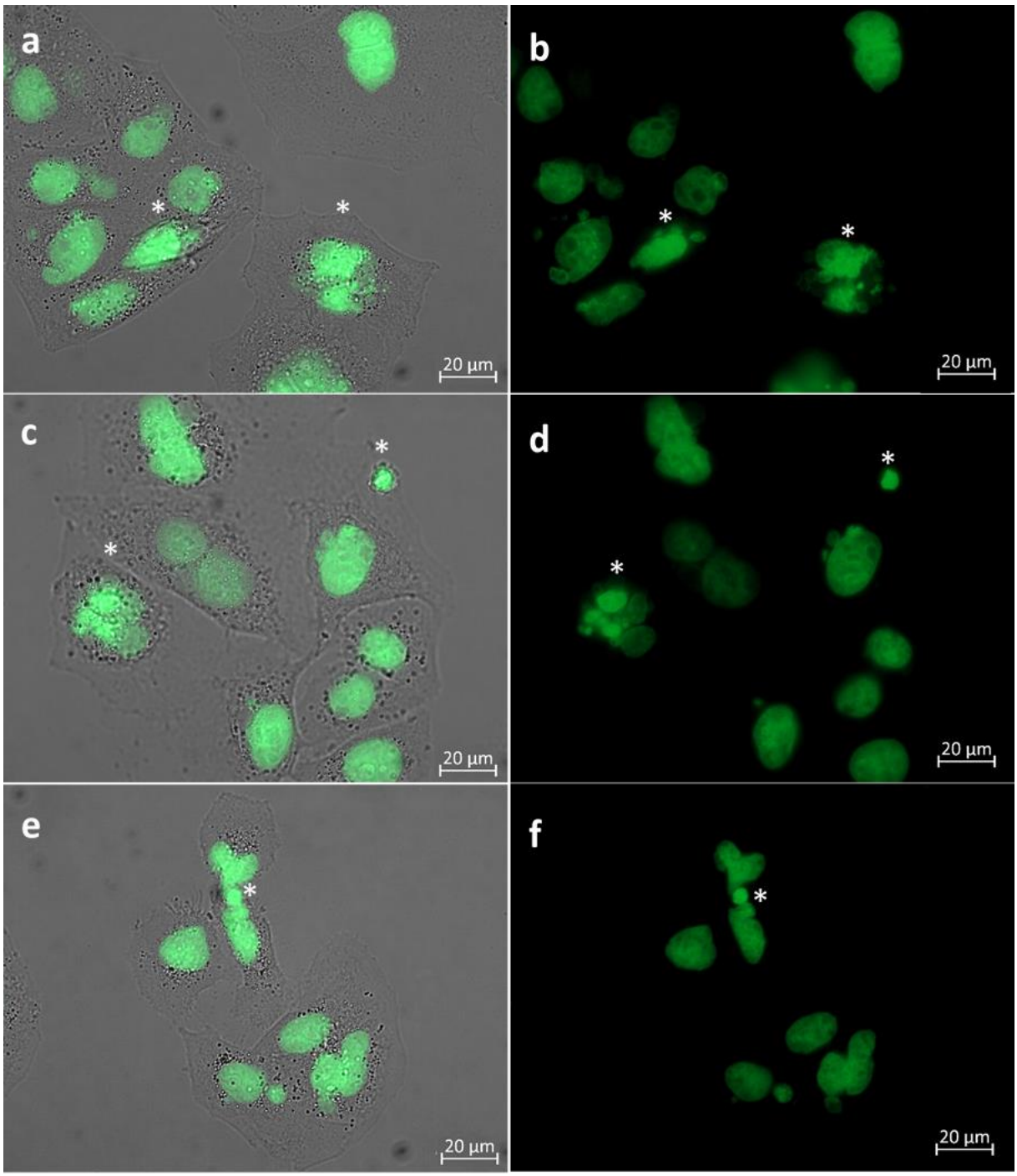

Figure 5. Drastic changes of cellular and nuclear morphology in living histone H2B-GFP permanently transfected He-La cells after irradiation with 30 Gy taken over 48 h; a-f – medium magnification; a, c, e - overlay of phase contrast and fluorescent images; b, d, f – same cells demonstrated in fluorescent regime only; a-f – initial appearance of polynuclear (Figure 5. a, c, e), apoptotic (Figure 5. c, d) and deformed (Figure 5. e) cells. Most probably Figure 5. a, b and Figure 5. e, f are mirroring the formation of cleaved and/or lobbed nuclei. Note asynchronous apoptosis of different nuclei within the same polynuclear cell (Figure 5. a-f, marked by stars).

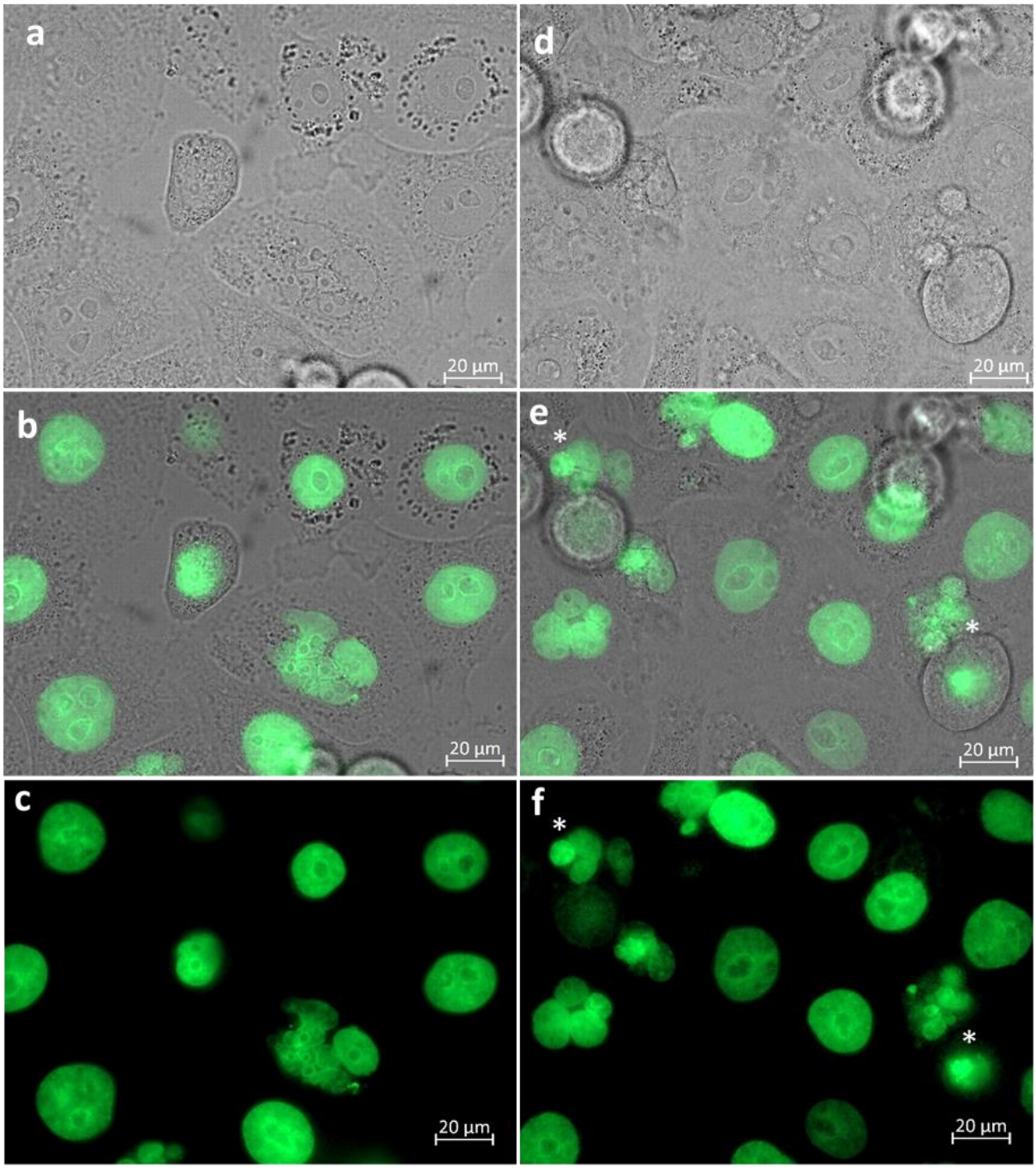

Figure 6. Drastic changes of cellular and nuclear morphology in living histone H2B-GFP permanently transfected He-La cells after irradiation with 10 Gy taken over 72 h; a-f – medium magnification; a, d – phase contrast only: appearance of intra-nucleolar light zones of different sizes; b-e – overlay of phase contrast and fluorescent images; c-f – same cells demonstrated in fluorescent regime only; b-f - the number of polynuclear and apoptotic cells dramatically increase. Asynchronous apoptosis is clearly seen (Figure 6. e, f marked by stars). Note profound PCC rings separating nucleolar territory from nucleoplasm. Even at medium magnification ICC clumps and their contact with PCC are well recognizable (Figure 6. f; see nucleus localized in the center of image).

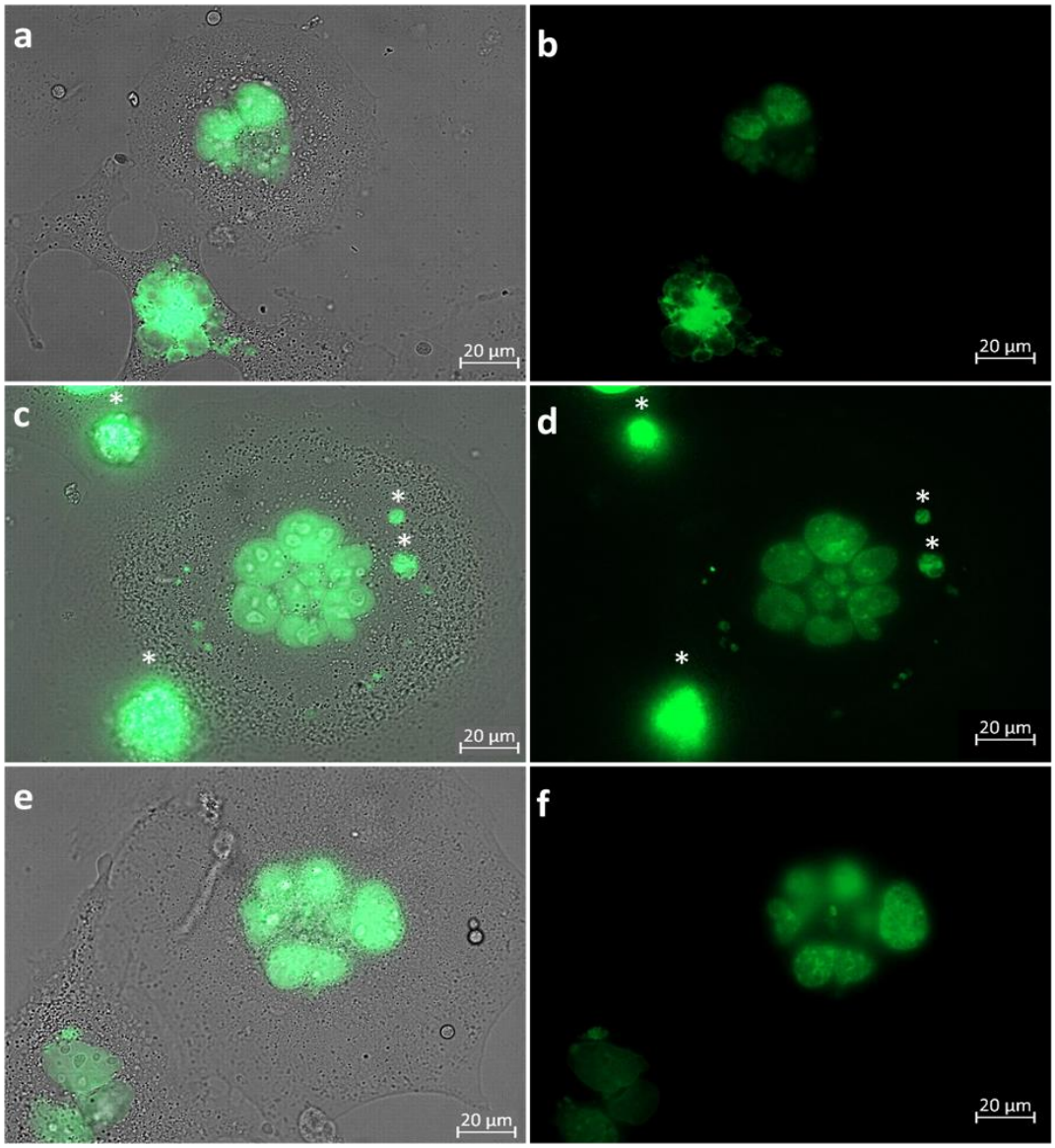

Figure 7. Gallery displaying drastic changes of cellular and nuclear morphology in living histone H2B-GFP permanently transfected He-La cells after irradiation with 30 Gy taken over 72 h; a-f – medium magnification; a, c, e – overlay of phase contrast and fluorescent images; b, d, f – the same cells taken using fluorescent regime only. This gallery shows massive appearance of giant polynuclear cells. Apoptotic cells marked by stars on Figure 7. c, d.

Through our 2D approach, we visualized: (i) gradual morphological changes and size variations in the nucleus, including deformation of nuclear contours; (ii) modifications in the nucleolar territory, involving alterations in the ICC network and PCC shell; (iii) the chronology of stages and potential mechanisms leading to polynuclear cell formation; (iv) asynchronous development of apoptosis-related changes in different nuclei of polynuclear cells. Together, it was revealed that post-irradiation, initially, ovoid nuclei transform into irregular shapes,

undergo drastic deformation or lobbying, and eventually fragment, resulting in the formation of polynucleated, dying cells. We did not find profound signs of cell division arrest, as different stages of mitosis (including its pathological forms) were also registered (**Figures 4.-8**).

According to time-dependent structural changes that develop in irradiation-damaged cells, we preferred to divide the whole period of post-irradiation time-lapse imaging into three stages: *stage 1* (0 - 24 h of the post-irradiation period), *stage 2* (24 - 48 h), and *stage 3* (48 - 72 h). Noteworthy, comparing the structural events over all three post-irradiation stages, we constantly specify much more profound changes in nuclear/nucleolar structure by treatment with 30 Gy regime than those of 10 Gy (compare Figure 4. and Figure 5.; Figure 6. and Figure 7.; Figures 8. a, b and Figures 8. b, c).

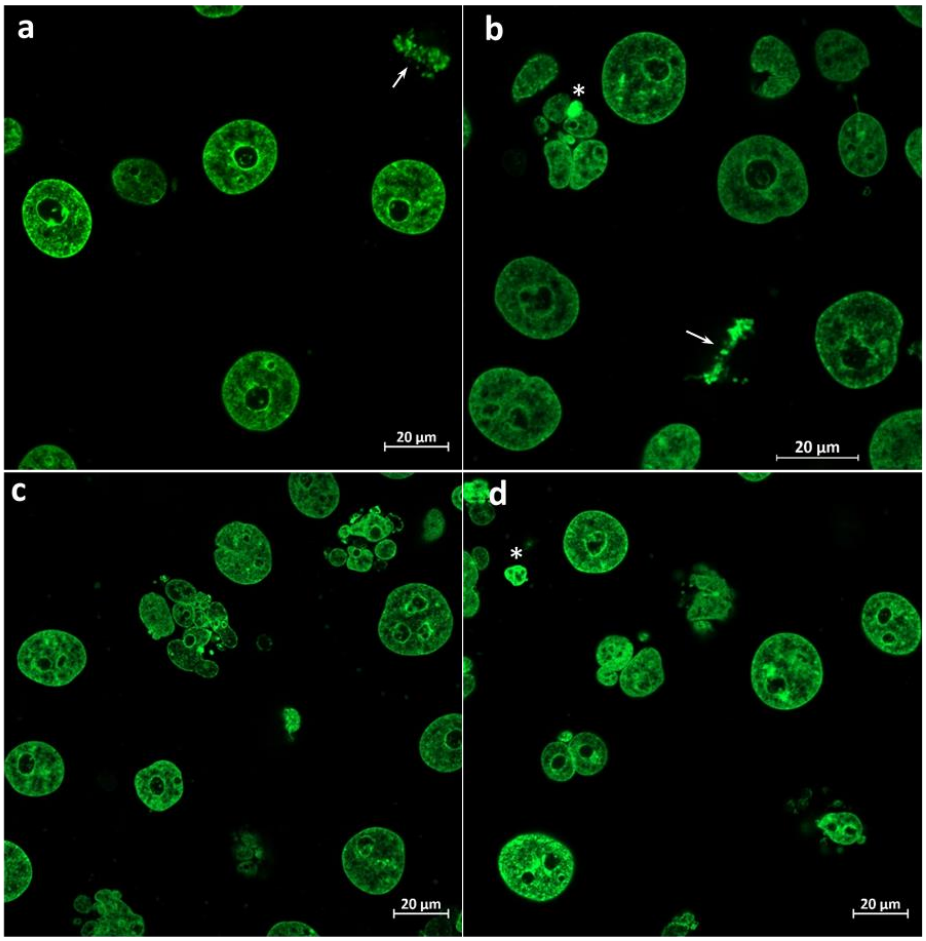

Figure 8. Changes in the structure and sizes of PCC and ICC as revealed at high magnification. a, b – fluorescent images taken using culture treated with 10 Gy over 48 h; c-d – fluorescent images correspond to treatment with 10 Gy over 72 h. Interestingly, that beside polynuclear cells (Figure 8. b-d) mitotic cells also present (Figure 8. a, b, arrows). At this stage of γ-irradiation all nucleoli contain coarse ICC inclusions that can look like clumps or reveal ring-shaped appearance (Figure 8. a, b; see upper nucleus). In all cells the PCC ring become especially prominent. Note also asynchronous apoptosis (Figure 8. b, d, marked by stars).

Stage 1: Post-irradiation changes over 24 hours. Related changes were analyzed using a 2D movie from time series at low and medium magnification. Individual LSM images reflecting different stages of post-radiation nuclear evolution were presented and analyzed in merged PC/fluorescent mode in order to better discriminate mononuclear and polynuclear cells. Correspondingly, key time points were identified and extracted for detailed analysis in galleries of individual/random sections, revealing cellular and nuclear shapes by treatment under 10 Gy and 30 Gy regimes. We concluded that during stage 1, culture maintained nuclear and nucleolar shape and structure without drastic changes over the 24-hour acquisition period, so that obtained pictures were similar to control ones. By this, mitotic cells could be detected quite often (corresponding images and movie are not shown).

Stage 2: Post-irradiation changes over 48 hours. During the 24 – 48 h post-irradiation period, the nuclear diameter progressively increased from 20.5 to 28 μm. However, the bulk of cells retain mononuclear appearance, while nuclei maintained roundish or ovoid shape with smooth outlines (Figure 4.). Mitotic cells that revealed structure very close to normal, were seen quite often (Figure 4. e, f). Over 48 h period, drastically deformed cells notably increase by treatment using 30 Gy regime, while polynuclear as well as apoptotic cells abundantly appear as displayed in Figure 5. Deformed nuclei exhibit deep invaginations, calculated from one to multiple. Apoptotic cells (including early stages) can be easily recognized due to dramatically enhanced nuclear brightness conditioned by increased chromatin compaction. Polynuclear cells can be observed very often. The number of polynuclear and apoptotic cells significantly grows to the end of imaging, i.e. after ~40 h of the post-irradiation period. In addition, different nuclei in these cells can reveal initial signs, indicating the asynchronous character of apoptotic changes. In parallel, the intra-nucleolar fluorescence becomes much brighter and more prominent than in previous samples due to the full disappearance of the ICC network and its transformation into large clumps, often being reshaped into a ring-like appearance (Figure 8. a). At the same time, we observed notable thickening of the PCC ring. Despite prominent cellular destruction, rare mitotic cells (mostly pathologic forms) could be seen.

Stage 3: Post-irradiation changes over 72 hours. The most profound effects of γ-irradiation, leading to apparent nuclear/nucleolar structural modifications and drastic changes in global cellular organization, were observed during the 48 h to 72 h period when we applied 10 Gy (Figure 6.) and 30 Gy (Figure 7.) irradiations. Consequently, a majority of the cells underwent a transformation from mono- to polynuclear forms. For example, by 30 Gy regime, massive apoptosis was detected starting from 56-60 hours into the post-irradiation period, whereas the number of wholly destructed/dead cells dramatically increase to the end of time-lapse imaging, i.e. to 70-72 h (Figure 7.). It should be specially noted that, upon comparing individual polynuclear cells, we concluded that the process of apoptosis occurs asynchronously across different nuclei within the same cell (Figures 6. e, f; 7, a, d; 8, b). At the same time, analyzing structural changes unraveled by imaging using phase contrast at medium magnification at 10 Gy regimes we registered emerging of large light zones inside nucleolus (Figure 6. a, d). At high magnification and fluorescent regime, it became clear that corresponding nucleolar modifications are concomitant with the appearance of extensive ICC zones that sometimes acquire the ring-shaped appearance. Prominent thickening of the PCC ring is also apparent (Figure 8.).

DISCUSSION

The molecular organization of the nucleolus is well documented at the molecular, genome, and proteome levels. Moreover, epigenetic mechanisms regulating r-genes expression have also been studied in detail. Consequently, over the past 30 years, the nucleolus has become recognized as a unique model for studying the spatial organization and functional state of mammalian r-genes, particularly in their functional and dynamic association with ribosome biogenesis and overall cell metabolism. Correspondingly, it is generally accepted that the sites of localization and transcription of r-genes, as well as processing of pre-RNA and pre-ribosome assembling factories organized as nucleolus, represent highly sensitive sensors of cellular stress [40-45]. Therefore, various chemical stress factors (including broadly used anticancer drugs) that inhibit different steps of ribosome biogenesis have been used as reliable tools to study structure-functional aspects of the nucleolus in compliance with cell metabolism [27, 35-39].

Conversely, while posing as an integral part of the nucleolus, the functional role of NAC still needs to be investigated despite recent data indicating its particular significance in the intra-nucleolar dynamics of NCs [27]. It is well established that, once formed, the nucleolus remains intimately associated with the physiological state of NAC. The structural remodeling of NAC can affect the spatial arrangement of active r-genes and the global organization of the nucleolar factories. For example, the contraction of NAC components drives the movement and fusion of FCs following the relocation of ICC/FC/DFC assembly from central regions to the nucleolar periphery and the incorporation of ICC into PCC [27].

Meanwhile, the structural and functional interplay between sophisticated systems, comprising giant tandems of r-genes, tightly folded and linked to unit NAC, remains completely unexplored. Most likely, NAC constituents do not contain r-genes due to the absence of specific accessory factors necessary for the maintenance of the template in an under-condensed/open state (e.g., UBTF). Hence, the absence of UBTF facilitate the keeping of the nucleosomal structure of ICC and PCC. How NAC responds to the action of DNA-damaging physical factors, particularly UV and radioactive exposure, remains largely unknown. Additionally, it is unclear how the transcriptional inactivation of r-genes, provoked by single-strand breakages, is reflected in the dynamics of nucleolar components. It seems much more problematic to understand whether NAC still retains the ability to condense and drive the movement of NCs while naDNA undergoes γ-irradiation breakage and degradation.

Therefore, the present study focuses on the reorganization of NAC, particularly ICC and PCC, under severe DNA damage induced by γ-irradiation. Accordingly, the primary goal of our study was to demonstrate the structural and functional interplay between γ-irradiation induced r-gene inactivation and large-scale modifications of intra-nuclear and intra-nucleolar structure with particular regard to possible territorial reorganization of NAC and related structures. The key findings are: (i) the dynamics of γ-irradiation-induced NAC inactivation mirror changes observed with AMD-induced rRNA synthesis inhibition. Under both irradiation regimes (10 Gy and 30 Gy), ICC structures coalesce and migrate towards PCC, forming more significant and prominent ICC clumps. This means that, despite severe naDNA damage, NAC, particularly ICC, retains the ability to contract and initiate the movement of NCs. The mechanisms underlying such a phenomenon, i.e., ICC and PCC contraction after single-strand breakage and

possible instant DNA repair, are completely obscured. (ii) As expected, a higher irradiation dose induces sufficiently rapid cellular response and more robust structural change, leading to cellular death via apoptosis. Thus, after treatment with 30 Gy, we revealed the bulk of highly deformed nuclei in both mononuclear and multinucleated cells, including apoptotic ones after 48 h. The same post-irradiation period by the 10 Gy regime shows visually nearly intact, roundish, and ovoid nuclei without any signs of nuclear deformation. In such cases, only increased nuclear diameter witnessed the influence of γ-irradiation upon cell/nuclear morphology. (iii) Post-irradiation changes over 24-72 hours enabled the revealing of the nuclear/nucleolar evolution stages and calculation of nuclear diameter changes. For this, we resorted to key time points that were identified for detailed analysis in galleries of individual sections, showing ICC and PCC changes in time. Because our study employs an approach involving both 2D LSM imaging of fixed cells and the time-lapse imaging we managed to visualize gradual morphological changes in the nucleus, modifications in the nucleolar territory (including ICC network and PCC ring), the chronology of stages leading to polynuclear cell formation, and asynchronous apoptosis-related changes. Although apoptosis in polynuclear cells was frequently registered after UV and γ-irradiation [46-51], up to date, there is no comprehensive explanation of underlying sub-cellular and molecular mechanisms. (iv) Importantly, our results demonstrate at least one of the possible sub-cellular mechanisms of polynuclear cell emergence. By this, the dynamics of this process develop in two steps. Initially, the formation of deep invaginations of the nucleus takes place that imparts a cleaved and/or lobbed shape to nuclei. During the next step, nuclei “disrupt” into separate fragments so that each lobe gives rise to individual nucleus. We observed two kinds of such a “cheeping of” process. If the lobe "engulfs" the nucleolus, nuclear disruption forms the nucleolated fragment. In opposite cases, fragments became anucleolated. Interestingly, apoptosis-associated changes develop asynchronously in both nucleolated and anucleolated nuclei. (v) Undoubtedly, one more intriguing issue worth further, more profound engagement is that even severe DNA damaging 30 Gr regime indicated the maintenance of naDNA to contract and drive nuclear and nucleolar dynamics; (vi) Another interesting nucleolus-related phenomenon deals with the emergence of large light zones known from classical studies as “nucleolini”, “clear zones” etc. These changes, which can be easily registered using the phase contrast approach, were considered a reliable criterion of r-genes inactivation, regularly observed when nucleolar functions were disturbed with chemical inhibitors. Typically, these optically and electron light micro-structures correspond to 1-3 giant FCs that became significantly enlarged due to the fusion of multiple but small individual FCs [27]. However, without specific labeling of r-genes transcription sites, it is challenging to determine whether enlarged light zones correspond to FCs or NVs.

In summary, the study contributes valuable insights into the structural changes in nuclear and nucleolar structure under severe DNA damage, highlighting the significance of NAC in nucleolar organization. The observed similarities between chemical inhibition and γ-irradiation effects emphasize the role of NAC in cellular responses to different stressors.

Acknowledgment

This project received the technical and financial support from the Director and Governing Board of New Vision University. The authors express heartfelt gratitude to the leadership and operational managers of New Vision University for their efficient assistance.

REFERENCES

[1]. Busch, H., Smetana, K. (1970) The Nucleolus. New York, Academic Press: 1-282;
[2] Smetana, K., Busch, H. (1974) The nucleolus and nucleolar DNA. In: Busch H, editor. The Cell Nucleus. New York, Academic Press: 73-147;
[3] Hadjiolov, A. (1985) The Nucleolus and ribosome biogenesis. In: Alfert, M, Beerman W, Goldstein, L, Porter, KR, Site P, editors. Cell Biology Monographs Wien, New York, Springer Verlag: 1-263;
[4] Thiry, M., Lafontaine D. (2005) Birth of a nucleolus: the evolution of nucleolar compartments. Trends in Cell Biology, 15:194-199;
[5] Boisvert, F. M., van Koningsbruggen, S. N., Navascues, J., Lamond, A. I. (2007) The multifunctional nucleolus. Nat Rev Mol Cell Boil, 8:574-585;
[6] Hernandez-Verdun, D., Roussel, P., Thiry, M., Sirri, V., Lafontaine, D. (2010) The Nucleolus: structure/function relationship in RNA metabolism. WIREs RNA, 1:415-431;
[7] Pederson, T. (2010) The nucleus introduced. Cold Spring Harb Perspect Biol, 10:1-16;
[8] Olson, M. O. J. (2011) The nucleolus: A nuclear body full of surprises. In: Olson M. O. J. editor. The Nucleolus. Protein Reviews, New-York, Dordrecht, Heidelberg, London: Springer, 15:5-17;
[9] Tafforeau, L., Zorbas, C., Langhendries, J. L., Mullineux, S. T., Stamatopoulou, V., Mullier, R. (2013) The complexity of human ribosome biogenesis revealed by systematic nucleolar screening of pre-rRNA processing factors. Molecular Cell, 51:539-551;
[10] Farley, K. I., Surovtseva, Y., Merkel, J., Baserga, S. (2015) Determinants of mammalian nucleolar architecture. Chromosom, 124:323-331;
[11] Pollock, C., Huang, S. The perinucleolar compartment. J Cell Biochem (2009), 107:189-193;
[12] Pollock, C., Daily, K., Nguyen, V. T., Wang, C., Lewandowska, M. A., Bensaude, O. (2011) Characterization of MRP RNA-protein interactions within the perinucleolar compartment. Mol Biol Cell, 22:858-867;
[13] Misteli, T. (2005) Concepts in nuclear architecture. Bioassays, 27:477-487;
[14] Ochs, R. I., Press, R. I. (1992) Centromere autoantigens are associated with nucleolus. Exp Cell Res, 200:339-350;
[15] McKeown, P. C., Shaw, P. J. (2009) Chromatin: linking structure and function in the nucleolus. Chromosoma, 118:11-23;
[16] Bartova, E., Horakova, A., Uhlirova, R., Raska, I., Galiova, G., Orlova, D. (2010) Structure and epigenetics of nucleoli in comparison with non-nucleolar components. J Histochem Cytochem, 58:391-403;
[17] Nemeth, A., Conesa, A., Santoyo-Lopez J., Medina I., Montaner D., Peterfia B. (2010) Initial genomics of the human nucleolus. PLOS Genetics, 6:1-10;
[18] Van Konningsbruggen, S., Gierlinski, M., Schofield, P., Martin, D., Barton, G. J., Ariyurek, Y. (2010) High resolution whole-genome sequencing reveals that specific chromatin domains from most human chromosomes associate with nucleoli. Molecular Biology Cell, 21:3735-3748;

[19] Nemeth, A., Langst, G. (2011) Genome organization in and around the nucleolus. Cell, 27:149-156;
[20] Stults, D. M., Killen, M. W., Pierce, H. H., Pierce, A. J. (2008) Genomic architecture and inheritance of human ribosomal RNA gene clusters. Genome Res, 18:13-18;
[21] Floutsakou, I., Agrawal, S., Nguyen, T. T., Seoighe, C., Ganley, A. R. D., McStay, B. (2013) The shared genomic architecture of human nucleolar organizer regions. Genome Res 23:2003-2012;
[22] Grob, A., McStay, B. (2014) Construction of synthetic nucleoli and what it tells us about propagation of subnuclear domains through cell division. Cell Cycle, 13:2501-2508;
[23] Derenzini, M., Thiry, M., Goessens, G. (1990) Ultrastructural cytochemistry of the mammalian cell nucleolus. J. Histochem Cytochem, 38:1237-1256;
[24] Thiry, M., Ploton, D., Menager, M., Goessens, G. (1993) Ultrastructural distribution of DNA within the nucleolus of various animal cell lines or tissues revealed by terminal deoxynucleotidyl transferase. Cell Tissue Res, 271: 33-45;
[25] Thiry, M., Goessens, G. (1996) The nucleolus during the cell cycle. In: Landes R.G. Company editor. Molecular Biology Intelligence Unit. Austin: Chapman and Hall: 1-146;
[26] Mosgoller, W. Nucleolar, (2003) Ultrastructure in Vertebrates. In: Olson MO editor. The Nucleolus. London: Plenum Publesher: 1-11;
[27] Tchelidze, P., Benassarou, A., Kaplan, H., O'Donohue, M. F., Lucas, L., Terryn, C., Rusishvili, L., Mosidze, G., Lalun, N., Ploton, D. (2017) Nucleolar Sub-Compartments in Motion during rRNA Synthesis Inhibition: Contraction of Nucleolar Condensed Chromatin and gathering of fibrillary centers are concomitant. PLOS one: 30: 2-37;
[28] Sudpraserta, W., Navasumrita, P., Ruchirawata, M. (2006) Effects of low-dose gamma radiation on DNA damage, chromosomal aberration and expression of repair genes in human blood cells., 209: 503-511;
[29] Zlobinskaya, G., Dollinger, D., Michalski, V., Hable, C., Greubel, G. Du., G., Multhoff, B., Roper, M., Molls, T. E., Schmid. (2012) Induction and repair of DNA double-strand breaks assessed by gamma-H2AX foci after irradiation with pulsed or continuous proton beams. Radiat Environ Biophys, 51: 23-32;
[30] Nishimaki, N., Tsukimoto, M., Kitami, A., Kojima, S. (2012) Autocrine regulation of γ-irradiation-induced DNA damage response via extracellular nucleotides-mediated activation of P2Y6 and P2Y12 receptors. DNA Repair: 11: 657-665;
[31] Ghorai, A., Bhattacharyya, N. P., Sarma, A., Ghosh, U. (2014) Radiosensitivity and Induction of Apoptosis by High LET Carbon Ion Beam and Low LET Gamma Radiation: A Comparative Study. Scientifica, 2014: 1-10;
[32] Juliana, H., Osaki, Espinha, Y. T., Magalhaes, Forti, F. L. (2015) Modulation of RhoA GTPase Activity Sensitizes Human Cervix Carcinoma Cells to γ-Radiation by Attenuating DNA Repair Pathways. OxIdative Medicine and Cellular Longevity 2016: 1-11.
[33] Zhoo, H., Zhuang, Y., Li, R., Liu, Y., Mei, Z., He, Z., Zhou, F., Zhou, Y. (2018) Effect of different doses of X-rey irradiation on cell apoptosis, cell cycle, DNA damage repair and glycolysis in He-La cells. Oncology Letters, 11: 42-54;
[34] Brunner, S., Varga, D., Bozó, R., R. Polanek, R., Tőkés, T., Szabó, E. R., Molnár, R., Gémes, N., Szebeni, G. J., Puskás, J. L., Erdélyi, M., Hideghéty, K. (2021) Analysis of Ionizing Radiation Induced DNA Damage by Superresolution dSTORM Microscopy. Pathology and Oncology Research, 27: 160-173;
[35] Reynolds, R. C., Montgomery P. O., Hughes, B. (1964) Nucleolar "caps" produced by actinomycin D. Cancer Res, 24: 1269-1277;

[36] Simard, R., Langelier, Y., Mandeville, R., Maestracci, N., Royal, A. (1974) Inhibitors as tools in elucidating the structure and function of the nucleus. In: Busch H, editor. The Cell Nucleus. New York: Academic Press: 447-487;
[37] Puvion-Dutilleul, F., Mazan, S., Nicoloso, M., Pichard, E., Bachellerie, J. P, Puvion, E. (1992) Alterations of nucleolar ultrastructure and ribosome biogenesis by actinomycin D. Implication for U3 snRNP function. Europ J Cell Biol, 58:149-162;
[38] Shav-Tal, Y., Blechman, J., Darzacq, X., Montagna, C., Dye, B. T., Patton, J. G. (2005) Dynamic sorting of nuclear components into distinct nucleolar caps during transcriptional inhibition. Mol Biol Cell, 16:2395-2413;
[39] Tchelidze, P., Kaplan, H., Terryn, C., Lalun, N., Ploton, D., Thiry, M. (2019) Electron Tomography Reveals Changes in Spatial Distribution of UBTF1 and UBTF2 Isoforms within Nucleolar Components during rRNA Synthesis Inhibition. Journal Structural Biology, 208(2): 191-204;
[40] Olson, M. (2004) Sensing cellular stress: another new function for the nucleolus? Sci STKE, 10.
[41] Maggi, L. B., Weber, J. D. (2005) Nucleolar adaptation in human cancer. Cancer Invest, 23:599-608;
[42] Mayer, C, Grummt, I. (2005) Cellular stress and nucleolar function. Cell Cycle, 4:1036-1038;
[43] Drygin, D., Rice, W. G., Grummt, I. (2010) The RNA polymerase I transcription machinery: An emerging target for the treatment of cancer. Annu Rev Pharmacol, 50:131-156;
[44] Michel, J., Nolin, F., Wortham, L., Lalun, N., Tchelidze, P., Banchet, V., Terryn, C., Ploton, D. (2019) Various Nucleolar Stress Inducers Result in Highly Distinct Changes in Water, Dry Mass and Elemental Content in Cancerous Cell Components: Investigation Using Nano-Analytical Approach. Nanoteranostics, 3:179-195;
[45] Potapova, T. A., Unruh, J. R., Conkright-Fincham, J., Banks, C. A. S., Laurence, F., Shneider, D. A., Gerton, J. L. (2023) Distinct states of nucleolar stress induced by anticancer drugs. eLife, 12:1-30;
[46] Braten, M., Banreed, H., Berg, K., Moan, J. (2000) Induction of multinucleated cells caused by UVA exposure in different stages of the cell cycle. J Photochem Photobiol B: Biology, 71(5): 620-626;
[47] Salucci, S., Burattini, S., Batistelli, M., Baldassarri, V., Maltarlo, M. C., Falcieri, E. (2013) Ultraviolet B (UVB) Irradiation-Induced Apoptosis in Various Cell Lineages in Vitro. Int. J. Mol. Sci., 14: 532-546;
[48] Lee, C. H., Wu, S. B., Hong, C. H., Yu, H. S., Wei, Y. H. (2013) Molecular Mechanisms of UV-indiced Apoptosis and its Effects on Skin Residential Cells: The Implication in UV based Phototherapy. Int. J. Mol. Sci., 14(3): 6414-6435;
[49] Salucci, S., Burattini, S., Curzi, D., Buentempo, T., Martelli, A. M., Zappa, G., Falcieri, E., Battistelli, M. J. (2014) Photochem Phtobiol B: Biology,141: 1-9;
[50] Mirzayans, R., Audrais, B., Scott, A., Wang, Y. W., Kumar, P., Murray, D. (2017) Int. J. Mol. Sci.,18(2): 360-379;
[51] Azzouz, P., Khan, M. A., Sweerey, N., Palaniar, N. (2018) Two-in one: UV radiation simultaneously induces apoptosis and NETosis. Cell Death Discovery, 4: 51-78.